Durability and weatherability of a styrene-ethylene-butylene-styrene (SEBS) block copolymer-based sensing skin for civil infrastructure applications

Austin Downey[a,b], Anna Laura Pisello[c,d], Elena Fortunati[e], Claudia Fabiani[c], Francesca Luzi[e], Luigi Torre[e], Filippo Ubertini[e], Simon Laflamme[f,g]

[a] *Department of Mechanical Engineering, University of South Carolina, Columbia, SC, USA*
[b] *Department of Civil and Environmental Engineering, University of South Carolina, Columbia, SC, USA*
[c] *CIRIAF Interuniversity Research Centre on Pollution and Environment "Mauro Felli", Perugia, Italy*
[d] *Department of Engineering, University of Perugia, Perugia, Italy*
[e] *Department of Civil and Environmental Engineering, University of Perugia, Perugia, Italy*
[f] *Department of Civil, Construction, and Environmental Engineering, Iowa State University, Ames, IA, USA*
[g] *Department of Electrical and Computer Engineering, Iowa State University, Ames, IA, USA*

Abstract

Structural health monitoring of civil infrastructure requires low-cost, scalable, long-term, and robust sensing technologies due to the size and complexity of the geometries under consideration. This paper investigates the durability and weatherability of a large area sensing skin engineered for civil infrastructure applications. This sensing skin is based on a soft elastomeric capacitor made of three thin layers based on an SEBS block co-polymer matrix. The inner layer is filled with titania and acts as the dielectric, while the external layers are doped with carbon black and work as the conductive plates. In this work, a variety of specimens, including the dielectric layer without the conductive plates, were fabricated and tested within an accelerated weathering chamber by simulating thermal, humidity, and UV radiation cycles. Beyond the accelerated weathering tests, a sensor deployed on a bridge in Iowa for six and a half years was removed from the field and analyzed in the laboratory. A variety of other tests were performed in order to characterize the specimens' mechanical, thermal, optical, and electrical performance. Additionally, strain sensitivity analyses were performed on specimens of interest. Results showed that titania inclusions improved the sensor dielectric's durability against weathering, while the carbon black doped conductive layers provided the skin sensor with a high level of durability and weatherability protection. The results in this work contribute to a better understanding of the degradation of SEBS-based matrices as well as the behavior of these skin sensors when deployed for the monitoring of civil infrastructure.

Keywords: Soft elastomeric capacitor, structural health monitoring, SEBS, durability, titania, titanium dioxide, TiO_2, weatherability, environmental degradation

1. Introduction

Structural health monitoring (SHM) is the automation of damage detection, localization, and characterization tasks in structures [1]. Effective SHM of civil infrastructure typically requires long-term monitoring strategies, because of the long life cycles coupled with harsh environmental conditions. One method to address the durability of sensors is embedment within structural components, as demonstrated in [2, 3, 4]. Another method to address sensor durability is to develop multifunctional structural materials that are capable of sensing their own condition, such as self-sensing con-

cretes [5], pavements [6], and bricks [7]. While both of these methods can provide long-term sensing capabilities for SHM systems, they are difficult to deploy and maintain compared with surface sensing techniques. Of interest to this paper are sensing skins, which have been recently proposed for monitoring large structural areas [8, 9, 10]. The authors have developed and demonstrated a low-cost, large-area, strain-sensitive parallel plate capacitor [11], termed soft elastomeric capacitor (SEC).

The vast majority of research efforts on sensing skin technologies have been focused on signals and scalability towards civil infrastructure applications, and there exists little information in the literature on the long term durability of these technologies. Nevertheless, some work has investigated the resilience of piezoelectric transducers to thermal cycles [12] and the long-term durability of fiber optic sensors in an aggressive marine environment [13]. In particular, the monitoring of civil infrastructure requires that the thin-film sensors are able to withstand harsh environmental conditions from changes in temperature, moisture, and ultraviolet (UV) radiation, while providing reliable measurements throughout the life of the structure. For the validation of any civil infrastructure measurement technology exposed to the elements, it is imperative to investigate its weatherability, because a monitoring campaign could last anywhere between one year (required to capture the thermal and humidity cycles) and the lifetime of the structure. The objective of this paper is to experimentally investigate the weatherability and durability of the SEC for long-term sensing applications.

The SEC is based on a styrene-ethylene-butylene-styrene (SEBS) block copolymer matrix. The SEBS matrix is selected due to its ease of manufacturing, elasticity, and strength [14]. However, a pure SEBS matrix has been shown to degrade when exposed to temperature, moisture, and ultraviolet light [15, 16]. To increase the durability of the sensor [17, 18] and the permittivity of the dielectric layer [19], the dielectric is doped with TiO_2 (titania or titanium dioxide). The addition of TiO_2 has been shown to increase UV stability in carboxylated styrene butadiene rubber latex film by retarding surface photo-oxidation [20]. The electrodes of the parallel plate capacitor are also constructed from an SEBS matrix, but doped with carbon black to provide conductivity in the SEBS matrix while providing mechanical compliance [21, 22]. The doping of carbon black into the SEBS matrix provides enhanced mechanical properties and thermal stability over pure SEBS [23] and improves the stability of SEBS against UV degradation [24].

In this paper, the long-term performance of the SEC technology is investigated, and provides the field with the following contributions: 1) a quantification of the increased durability and weatherability provided by the filling of the SEBS matrix with TiO_2; 2) the demonstration that the conductive plates doped with carbon black provide a protective layer for the inner dielectric that increases the durability of the SEC sensor; and 3) the assessment of the sensor's capability to retain its strain sensitivity throughout the considered lifespan. The rest of the paper is organized as follows. First, the SEC sensing technology is introduced, including the fabrication process and electromechanical model. After, the experimental methodology is described, followed by a presentation of results and discussion.

2. Soft Elastomeric Capacitor Technology

2.1. Sensing Skin Fabrication

The SEC, shown in figure 1, is a highly scalable thin-film strain sensor engineered for structural health monitoring of large-scale structural components. The sensor is a parallel plate capacitor and as such is composed of three layers, where two electrically conductive electrodes are separated by a dielectric as illustrated in the expanded view of the SEC in figure 1(b). The scalability of the SEC arises from its simple and low-cost fabrication process. First, SEBS is dissolved using a reagent grade toluene, after which TiO_2 is dispersed using an ultrasonic tip (D100 Sonic Dismembrator manufactured by Fisher Scientific). The solution is drop-casted to create the dielectric onto a 75×75 mm^2 glass slide covered with a non-porous Polytetrafluoroethylene (PTFE) coated fiberglass fabric (Release Ease 234 TFNP by Airtech International) and the toluene let evaporate. Next, a conductive paint is fabricated by mixing carbon black (Printex XE 2-B) into another dissolved SEBS solution, forming a conductive paint. This paint is applied to either side of the dielectric to create the electrodes of the parallel plate capacitor. Lastly, copper contacts with conductive adhesives are added to each electrode and a thin layer of the conductive paint is added onto the copper contact to ensure a good connection between the copper and the conductive

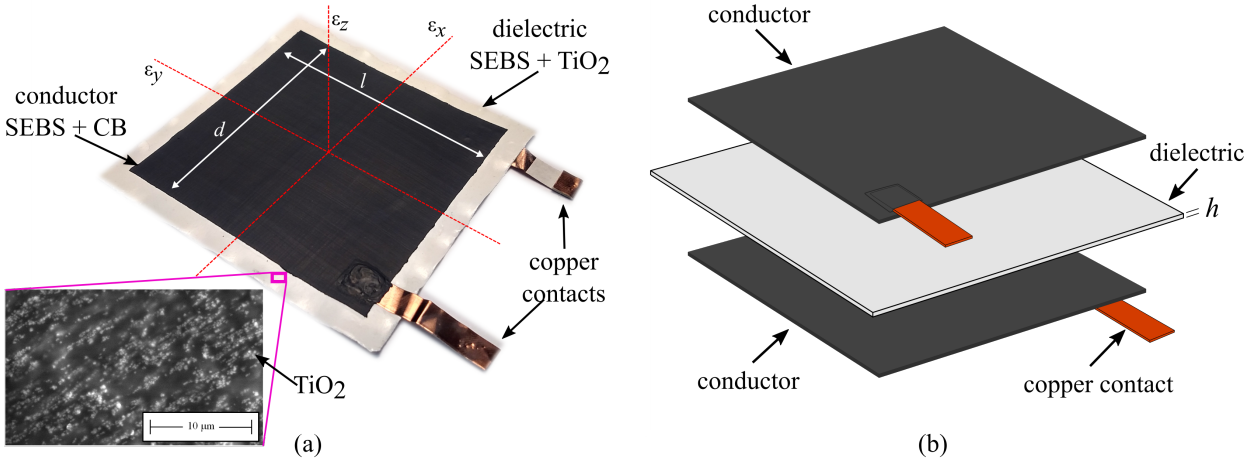

Figure 1: The soft elastomeric capacitor (SEC): (a) picture of a sensor used in this study with key components annotated with the inset showing a scanning electron microscope image of the dielectric; (b) an exploded view of the sensor geometry with key components annotated.

plates, as shown in figure 1(a). A more detailed description regarding the fabrication processes of the SEC sensors can be found in references [11] and [25].

The sensor's strain sensing principle is based on a measurable change in its capacitance provoked by a change in its geometry. By deploying the SEC along its plane, this change in geometry arises from a strain in the monitored surface. Its deployment is typically conducted using a commercial two-part epoxy and pretensioning the sensor during installation enabling the measurement of both compressive and tensile strain. The capacitance, C, of an SEC can be approximated using

$$\Delta C = e_0 e_r \frac{\Delta A}{\Delta h} \tag{1}$$

where $e_0 = 8.854$ pF/m and e_r are the vacuum permittivity and the polymer relative permittivity, respectively, A is the overlapping area of the conductive electrodes ($d \cdot l$ in figure 1(a)), and h is the thickness of the dielectric (figure 1(b)). The static [11] and dynamic [25] sensing capabilities of the SEC have been investigated. In brief, assuming small strains, equation (1) can be written as a change in capacitance (ΔC):

$$\frac{\Delta C}{C} = \frac{\Delta d}{d} + \frac{\Delta l}{l} - \frac{\Delta h}{h} \tag{2}$$

where it can be noted that $\Delta d/d$, $\Delta l/l$, and $\Delta h/h$, can be expressed as strain components ε_x, ε_y, and ε_z, respectively. Assuming a plane stress condition, $\varepsilon_z = -\nu(\varepsilon_x + \varepsilon_y)/(1-\nu)$, a relative change in capacitance ΔC can be related to a change in the sensor's geometry as

$$\frac{\Delta C}{C} = \lambda(\varepsilon_x + \varepsilon_y) \tag{3}$$

where ν is the sensor material's Poisson's ratio taken as $\nu \approx 0.49$ [26]. In Eq. 3, $\lambda = 1/(1-\nu) \approx 2$ represents the gauge factor of the sensor. A key advantage of the SEC is its capability to measure additive strain, as shown in equation (3). In addition to these material-based studies, the SEC has been experimentally investigated for structural health monitoring specific applications, including: fatigue crack detection [27]; full field strain map reconstruction [28]; and damage detection and localization in a model wind turbine blade under aerodynamic loading [29].

3. Experimental methodology

Various specimens were fabricated using varying concentrations of TiO_2 in the sensors' dielectric layer (0%, 5%, 10%, and 15% by volume). This work studies both the dielectric and the SEC sensor itself under a variety of induced environmental conditions simulated within an accelerated weathering chamber (QUV tests) where the focus of this research is the development of a mechanically robust sensor that is able to withstand the thermal,

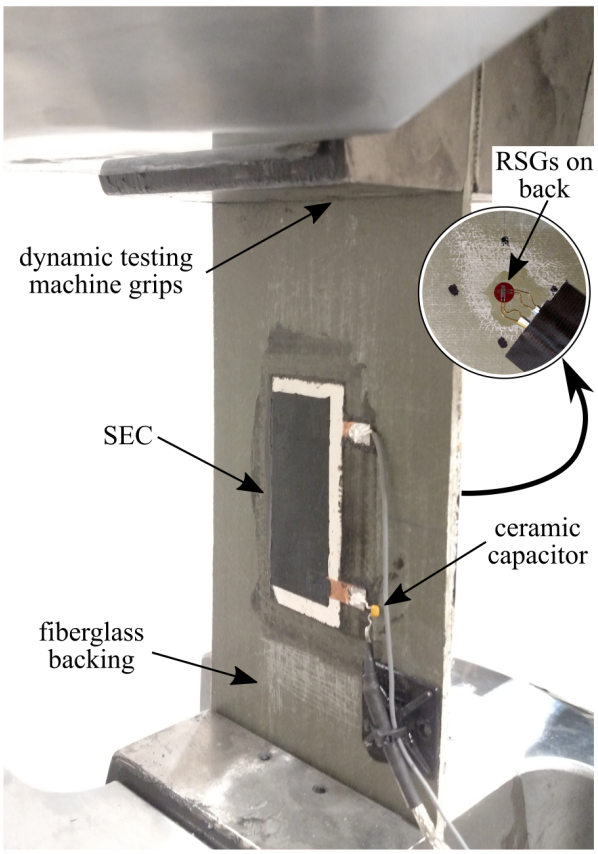

Figure 2: Experimental test setup of an SEC specimen attached to a fiberglass plate mounted in the dynamic testing machine. The inset shows the two-element RSG attached to the back of the fiberglass plate behind the SEC.

humidity, and UV radiation cycles that the SEC sensor could experience in an infrastructure monitoring application. Due to the small thickness of the conductive layer (0.02-0.6 mm) and the fact that it is painted onto the SEC during manufacturing, the conductive layers were not tested individually. Rather, the conductive layer's capability to provide a protective layer for the dielectric was investigated through testing of the SEC sensors. In order to provide consistent strain transducing capabilities, it is important to verify that the capacitance of the sensor does not vary significantly with age. The accelerated weathering tests utilized in this study include simulated thermal, humidity, and UV radiation cycles. Once completed, a series of tests were performed in order to characterize the sensors capacitance, mechanical, and thermal performance in addition to their solar reflectance at 0, 1, 7, 15, and 30 days. Additionally, strain sensitivity and linearity tests were performed on the sensors with 0 days and 30 days of accelerated aging. In addition to the accelerated aging tests, an SEC sensor that was deployed on a 2-lane highway bridge in Iowa in 2011 was retrieved and its dynamic sensing capabilities were inspected.

3.1. Investigated specimens

This study utilized 25 SEC sensors and 20 dielectric specimens. Of the SEC sensors, 24 were fabricated for this study and 1 was removed from a 2-lane highway bridge located in Iowa, USA, after being deployed for six and a half years. Except for the sensor removed from the South Skunk River Bridge, the specimens sat for a total 12 months between their initial fabrication process and final strain sensitivity investigation, with the accelerated aging taking place approximately six months after fabrication. During this 12-month period, the specimens were left in a laboratory environment at room temperature. All SEC sensors and the dielectric specimens measured 75 $\times$ 75 mm^2 while the SEC sensors had a sensing area of 65 $\times$ 65 mm^2. This reduction in the sensor's sensing area is due to the dielectric that extends past the edges of the conductive plates, as shown in figure 1(a). When measured as sitting flat on a table in a relaxed state, the SEC sensors exhibited an average capacitance of 535 pF with a standard deviation of 30 pF. Eight SECs were used for control and 16 were used as specimens for the accelerated aging tests. For the dielectric layers (including those of the SEC sensors), four different concentrations of TiO_2 were investigated: 0% (pure SEBS), 5%, 10%, and 15% TiO_2 by volume. During fabrication, it was found that the dielectric with 0% TiO_2 was unable to withstand the application of the conductive paint, because the conductive paint would dissolve through the pure SEBS matrix of the dielectric creating a conductive pathway from one electrode to another, therefore disabling the sensors. It follows that the 0% TiO_2 sample is not considered for the SEC specimens. Material specimens were cut from both the SEC and dielectric specimens for the mechanical testing, as needed, therefore, the final forms of the specimen were half of the SECs original size, as presented in the experimental setup of the strain sensitivity analysis shown in figure 2.

Lastly, a sensor deployed on a bridge during a preliminary investigation into the use of the SEC for SHM, work published in reference [30], was removed and tested in a laboratory setting. The sen-

sor was deployed onto the underside of a concrete deck on the South Skunk River Bridge, located in Ames, Iowa, USA. The bridge is shown in figure 3(a) while the installed sensor is shown in figure 3(b). The sensors were installed in December 2011 and retrieved in June 2018 for a total deployment time of 6.5 years. During this time, the sensor experienced a maximum high temperature of 37.7 °C on July 23rd and 25th 2012 and maximum low temperature of -30 °C on both February 5th, 2015 and January 1st, 2018 [31]. Furthermore, during the summer of 2016, the steel components on the South Skunk River Bridge were painted and the SEC received a layer of paint as a result of overspray. During this painting procedure, the maintenance crews ripped out all of the wiring to the SEC and removed the data acquisition system shown in figure 3(b). Therefore, only the sensor material (without any copper contacts) remained on the bridge. The sensor after being removed from the bridge, with new copper contacts attached to both sides of the sensors, is shown in figure 3(c). For testing, the green paint was removed from the sensors by repeatability applying and removing a cloth-backed tape (duct tape) from the painted side of the SEC. Once the paint was removed, the SEC was cut in half to remove a portion of the sensor with mechanical damage and to match the geometry of the previously tested specimens. A thin layer of conductive paint was applied to the top of the SEC sensor to ensure a good electrical connection between the copper contact and the sensor. As before, a two-element RSG was attached to the fiberglass plate behind the SEC. The experimental setup is shown in figure 3(d).

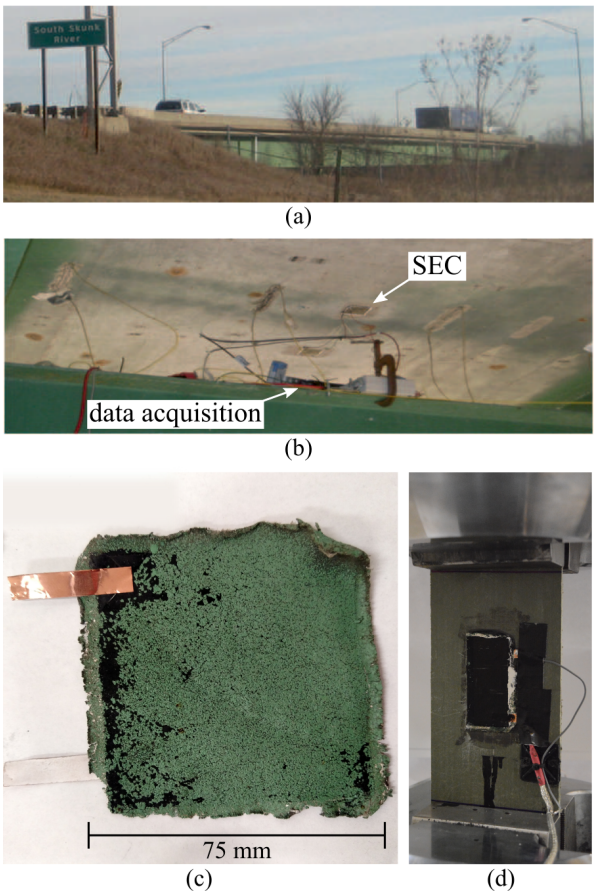

Figure 3: SEC sensor deployed under the deck of the South Skunk River Bridge, IA, in 2011, showing the: (a) South Skunk River Bridge; (b) SEC adhered to the bridge before the repaint; (c) SEC sensor as removed from the bridge (with new contacts added); and (d) SEC sensor attached to a fiberglass substrate for testing.

3.2. Accelerated weathering

Controlled accelerated weathering was used to investigate the durability of both the SEC sensor and dielectric specimens. This controlled experimental investigation was intended to quantify the sensors' capability to withstand the combined effects of thermal stress, high levels of humidity, and damaging UV solar radiation. The different specimens were placed in a QUV machine (QUV Accelerated Weathering Testes, Q-Lab), and the aging test was carried out following ASTM D 4329-99 [32], following the operative procedure described in ASTM G 154-06 [33]. According to the standard procedure, the specimens were alternately exposed to repeated cycles of UVA radiation (340 nm, energy of 0.77 W/m^2) at 50 °C for 8 hours followed by 2 hours in a humid condition (100 RH%) at 40 °C then 2 more hours at 20 °C (100 RH%). After 1, 7, 15, and 30 days of exposure, the effect of the accelerated weathering tests on the different specimens were evaluated in terms of visual observations, color variation, mechanical responses by tensile test and degradation properties by thermogravimetric analysis. Also, the control specimens and those that experienced 30 days of accelerated weathering were experimentally tested to assess their strain sensitivity and linearity. There is no standard on the equivalence between QUV tests and real-world exposure times as one year of exposure in an urban environment may be ten times more damaging than a year of exposure in a rural setting [34].

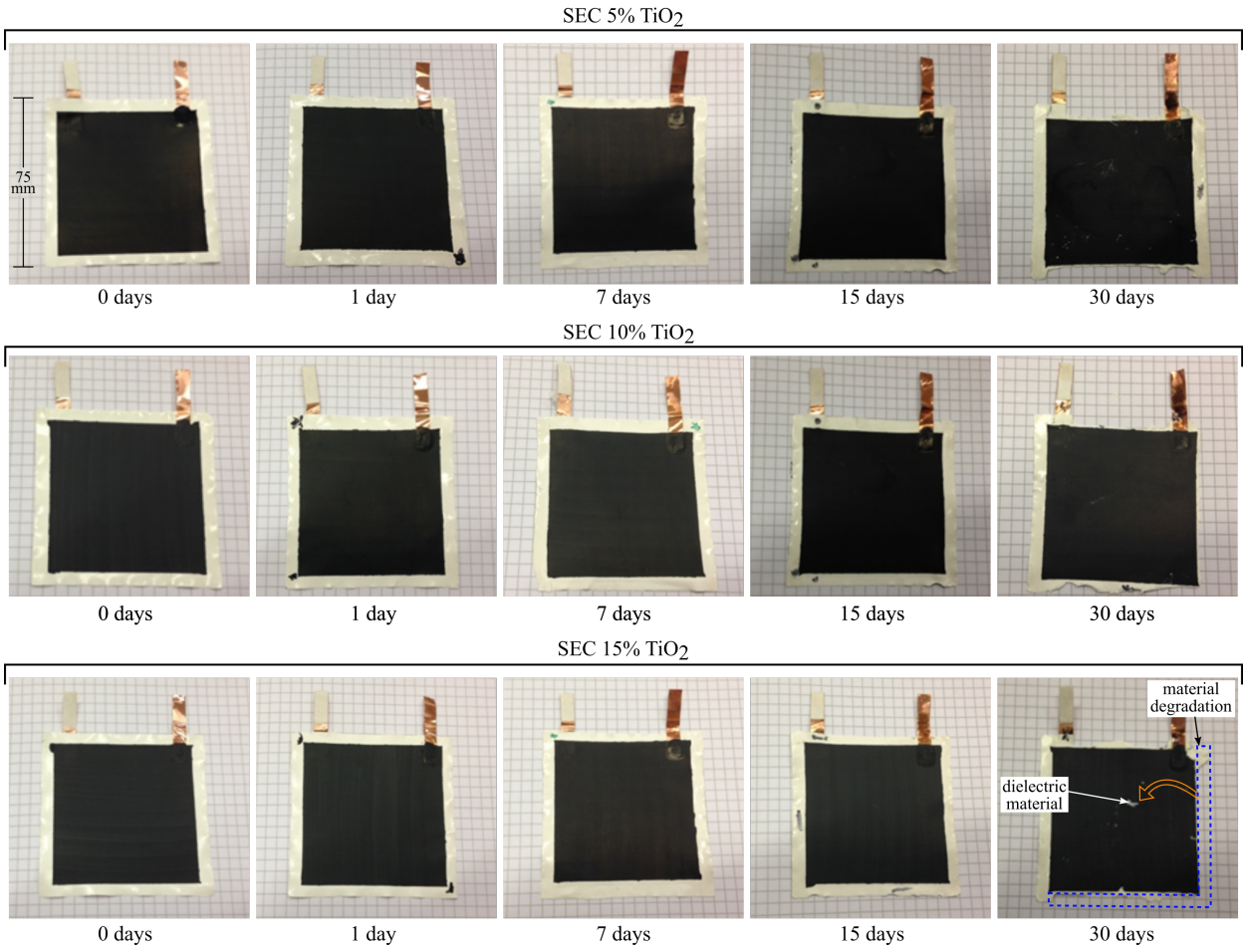

Figure 4: Accelerate aging of SECs with dielectric with that consist of 5, 10, and 15 % TiO_2 at 0, 1, 7, 15, and 30 days of QUV aging.

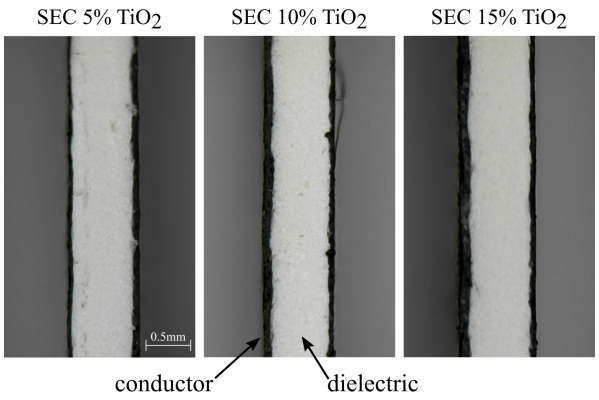

Figure 5: Optical images of the SEC cross sections after 30 days of accelerated aging.

3.3. Sample characterization

Sample characterization was performed through a series of mechanical, thermal, electrical, optical, and strain tests both before and after the accelerated aging exposures where the mechanical characteristics of the specimens were evaluated under tensile loadings. A material testing machine (Lloyd Instrument LR 30) with a 500 N load cell at room temperature was used to test five rectangular specimens (50 mm × 5 mm). A cross head speed of 1.66 mm/sec along with an initial gauge length of 25 mm were used during testing. The tensile strength (σ_r) and strain at rupture (ε_r) were measured during testing while the Young's modulus (E) was obtained from the specimens' stress-strain curves. The mechanical characterization tests were each conducted from multiple samples cut from the same specimen. Five samples were cut from each specimen for the

unaged samples and three samples for each of the aged specimens.

Thermogravimetric analysis (TGA) was used to quantify the specimens' thermal degradation, before and after the UV weathering. This was done using a TGA system (Seiko Exstar 6300). TGAs were performed using the following test parameters: 10 mg weight specimens, nitrogen flow rate of 250 ml/min, and temperatures ranging from 30 °C to 800 °C with a heating rate of 10 °C/min. The residual mass from thermogravimetric curves of different mixes that experienced varying amounts of accelerated aging were evaluated in order to study the effect of weathering on the degradation behavior of the studied materials.

Visual comparisons were recorded using digital photographs of the different specimens before and after the exposure to the accelerated aging tests. Additionally, the color changes of the studied materials were examined with a spectrophotometer (CM-2300d Konica Minolta, Japan). Data was acquired using the SCI 10/D65 method with CIELAB color variables, as defined by the International Commission on Illumination [35]. The ΔL*, Δa*, and Δb* parameters and gloss level were determined by placing the specimens on a standard white plate.

Optical characterization was performed by means of a solar spectrophotometer incorporating an integrating sphere. The tests were performed according to the international test method reported in ASTM E 903-96 [36]. This ASTM describes the procedure to perform measurements of spectral near normal-hemispherical reflectance over the spectral range of 300-2500 nm with a lab instrument. In typical applications where the solar reflectance values are are of interest, these values are calculated by weighting wavelength with respect to reference solar spectra (according to reference values [37]). However, as this study focuses on the material characterization of the specimens rather than its capability to reflect solar radiation, a simple measurement technique is implemented and the terrestrial solar irradiance distribution is not evaluated. The spectrophotometer (SolidSpec-3700) was equipped with a 60 mm-diameter integrating sphere with a wavelength accuracy of 0.1 nm. The spectrophotometer used a double beam scheme with coated optics. During testing, the spectral 100% and the zero lines were recorded at first to be kept as reference for the whole characterization campaign. Thereafter, the materials were tested and the reflectance values were obtained. This procedure is consistent with literature [38].

The capacitive stability of the SEC sensors was investigated by measuring the capacitance of the sensor both before and after the accelerated aging processes. Capacitance was measured using an LCR meter (875B manufactured by BK precision). Capacitance tests where performed at room temperature using a frequency of 1K Hz and a parallel capacitance mode. The capacitance for the 15 SEC specimens used for the durability investigation was measured. These measurements were also taken after 1 year with sensors being subjected to either 0, 1, 7, 15, and 30 days of QUV aging. To accommodate for the fact that materials were cut from each of these specimens for material testing, the capacitance of sections of the sensors was measured (e.g. a 35 $\times$ 75 mm^2) and adjusted using Equation 1. Once these adjustments were made, a capacitance for the sensors after aging could be estimated.

Strain sensitivity analysis was performed for both the aged SEC sensors specimens that experienced 30 days of accelerated aging and the control specimens. Due to materials specimens being taken from the SEC specimens for the prior investigations, only half of each aged sample remained. For consistency, the control specimens were cut down to the same dimensions as the specimens that underwent accelerated aging. These specimens were then mounted unto a fiberglass plate for testing, as presented in figure 2. Capacitance data from the SECs was acquired using a custom built capacitance-to-digital converter connected to a laptop computer. A ceramic capacitor was added to one contact of the SEC sensors to adjust the measured capacitance value of the SEC sensor, this offset was accounted for in post-processing. To validate the SEC sensors, a two-element RSG (model #FCA-5-350-11-3LJBT, manufactured by Tokyo Sokki Kenkyujo) was mounted unto the back of the fiberglass to measure the additive strain directly behind the sensor. The SEC specimens were tested using a servo-hydraulic dynamic testing machine. A displacement controlled load of 1.80 mm at 0.25 Hz was used. The strain values for the SEC sensors were calculated using the gauge factor of 2 as presented in equation 3 while the RSG strain values were obtained by adding the outputs of two RSG sensors ($\varepsilon_{\mathrm{x}} + \varepsilon_{\mathrm{y}}$).

Lastly, a strain sensitivity analysis was performed for the sensor removed from the South Skunk River Bridge. In an effort to validate the SEC against

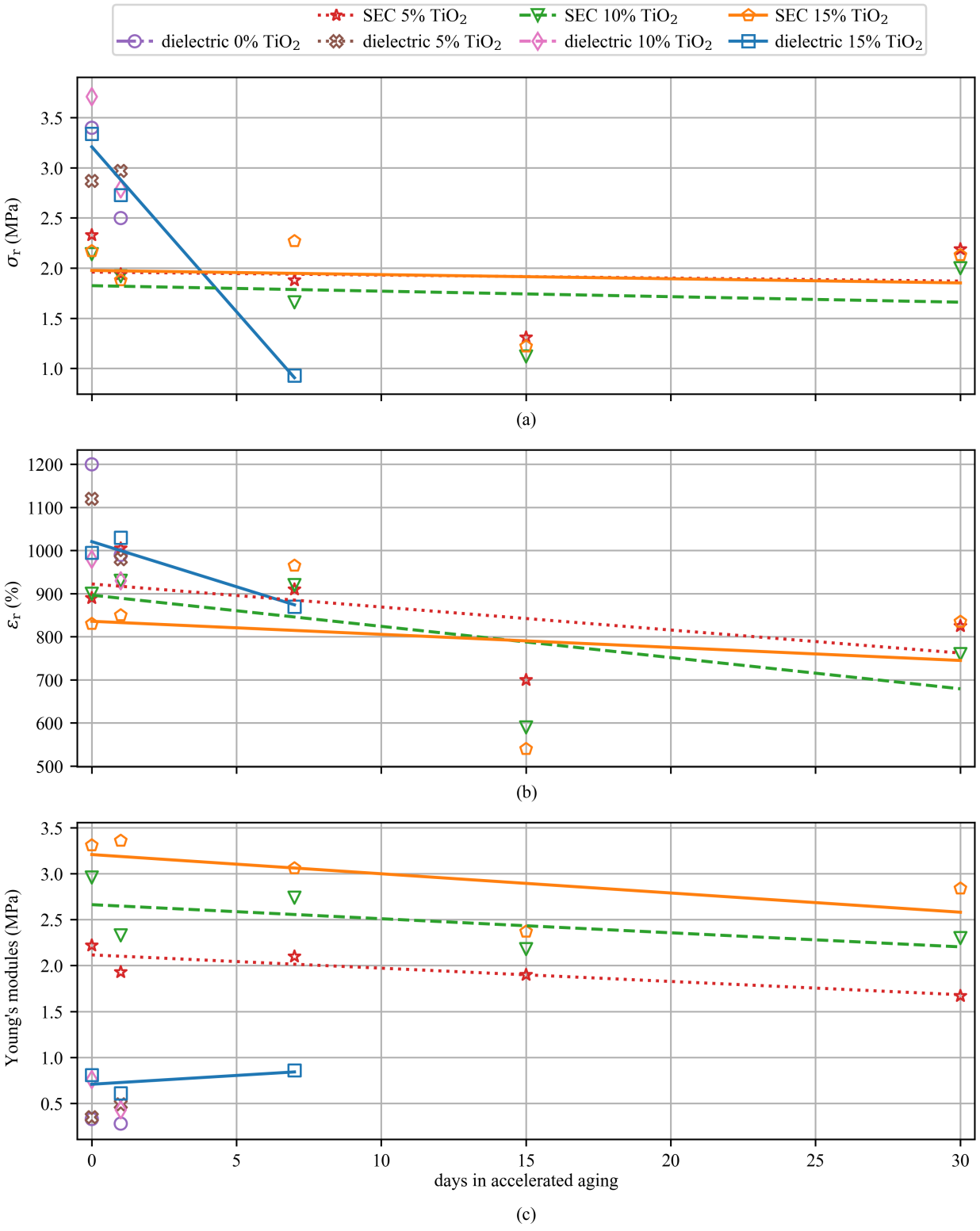

Figure 6: Mechanical properties of the SECs and dielectrics, with different concentrations of TiO_2 (dielectric layer), after accelerated aging: (a) tensile strength; (b) strain at rupture; (c) Young's modulus.

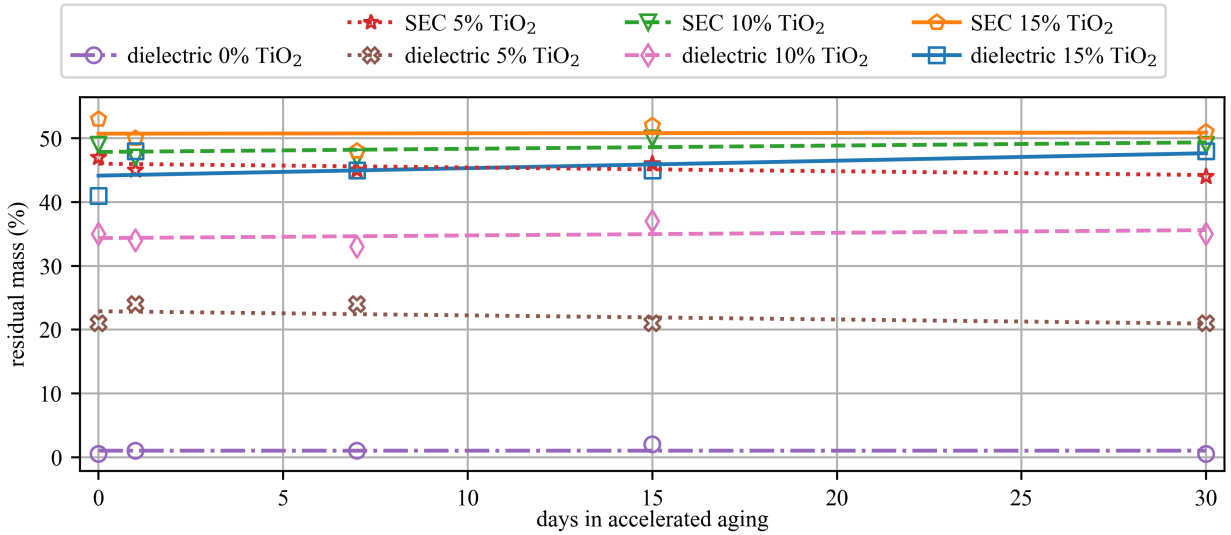

Figure 7: Residual masses of the SECs and dielectrics, with different concentrations of TiO_2 doped into the dielectric layer, after accelerated aging.

previously published data, an experimental procedure was developed where the fiberglass plate was excited at frequencies of 1.07 Hz, 2.91 Hz, and 4.20 Hz. These frequencies were chosen to mimic the bridge's dynamic response as presented in [30], that the sensor was previously capable of capturing. During testing, resistive strain gauges (RSGs) mounted on the back of the fiberglass plate were used to validate the SEC's strain transducing capabilities.

4. Results and Discussion

4.1. Visual analysis

Pictures of the various SEC specimens after undergoing accelerated aging are presented in figure 4. These photographs were taken after the specimens were removed from the environmental test chamber and before material specimens were cut from the SEC sensors for mechanical testing. For all three material formulations, the SEC sensors were found to maintain both their general appearance and structural integrity after the accelerated aging tests. In comparison, any unprotected portions of the dielectric layer around the outside of the SEC sensor was found to greatly degrade. Care had to be taken when removing the unprotected portion of the SECs from their aluminum backing plates. However, once the dielectric was detached from the test plate, the SEC could be easily removed. After 30 days of accelerated aging, any unprotected portions of the sensors dielectric greatly degraded and maintained very little structural integrity and some pieces fully separated from the dielectric layer and fell onto the carbon-black-based conductor as denoted by the arrow in the lower right-hand subset of figure 4. No degradation or holes were found in the carbon black doped conductor layer of the SEC sensors and this conductive layer was found to provide an excellent protective layer for the dielectric. This high level of protection for the dielectric layer is further demonstrated by the optical images of sample cross sections that were subjected to 30 days of accelerated aging presented in figure 5.

4.2. Durability analysis of mechanical and thermal behavior of the specimens

Figure 6 shows the mechanical properties of the SECs and dielectric layers after accelerated aging with various levels of TiO_2 in the dielectric layer. The material properties were tested without any accelerated aging (0 days) and after 1, 7, 15, and 30 days of exposure. Figures 6(a) and 6(b) are the measured values of tensile strength and strain at rupture, while figure 6(c) reports the calculated Young's modulus. Table 1 reports the mean and standard deviation in the measurements for all three mechanical properties investigated. After accelerated aging, some specimens were too fragile

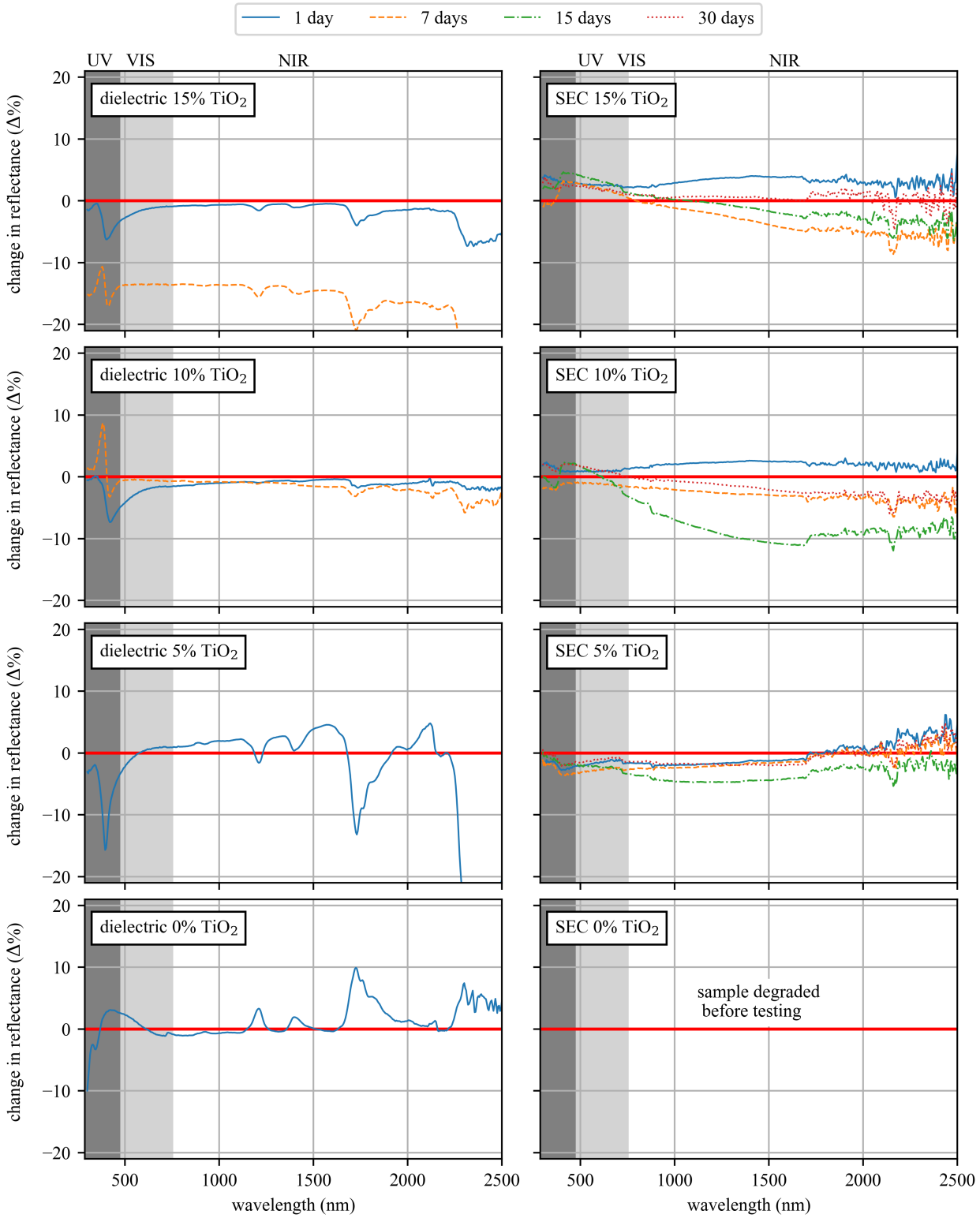

Figure 8: Change in solar reflectance of the dielectric and the SEC sensor exposed to 1, 7, 15, and 30 days of weathering procedure with respect to the same reference specimens, e.g. the dielectric and of the SEC sensors with 0 days of aging (SR_{day} - SR_{day-0}) / SR_{day-0}.

Table 1: Mean and standard deviation values for the tensile strengths at rupture (σ_r), strains at rupture (σ_r), and the calculated material modulus presented in figure 6.

specimens	σ_r (MPa)	σ_r (%)	material modulus (MPa)
no accelerated aging			
dielectric 5% TiO_2	2.87±0.28	1120±100	0.35±0.04
dielectric 10% TiO_2	3.71±0.52	980±25	0.76±0.08
dielectric 15% TiO_2	3.34±0.76	995±110	0.81±0.13
SEC 5% TiO_2	2.33±0.17	890±65	2.22±0.20
SEC 10% TiO_2	2.14±0.09	900±80	2.96±0.22
SEC 15% TiO_2	2.17±0.13	830±40	3.31±0.83
1 day of accelerated aging			
dielectric 5% TiO_2	2.97±0.34	980±50	0.49±0.03
dielectric 10% TiO_2	2.79±0.12	930±45	0.43±0.06
dielectric 15% TiO_2	2.73±0.26	1031±45	0.61±0.16
SEC 5% TiO_2	1.94±0.29	1005±80	1.93±0.14
SEC 10% TiO_2	1.92±0.36	930±70	2.33±0.28
SEC 15% TiO_2	1.88±0.24	850±75	3.36±0.61
7 days of accelerated aging			
dielectric 15% TiO_2	0.93±0.02	871±25	0.86±0.20
SEC 5% TiO_2	1.88±0.30	910±20	2.10±0.43
SEC 10% TiO_2	1.66±0.30	920±100	2.74±0.42
SEC 15% TiO_2	2.27±0.11	965±30	3.06±0.44
14 days of accelerated aging			
SEC 5% TiO_2	1.31±0.14	700±30	1.90±0.05
SEC 10% TiO_2	1.12±0.10	590±50	2.18±0.10
SEC 15% TiO_2	1.22±0.11	540±20	2.37±0.04
30 days of accelerated aging			
SEC 5% TiO_2	2.19±0.26	825±55	1.67±0.25
SEC 10% TiO_2	2.00±0.37	760±40	2.30±0.2
SEC 15% TiO_2	2.13±0.21	835±50	2.84±0.30

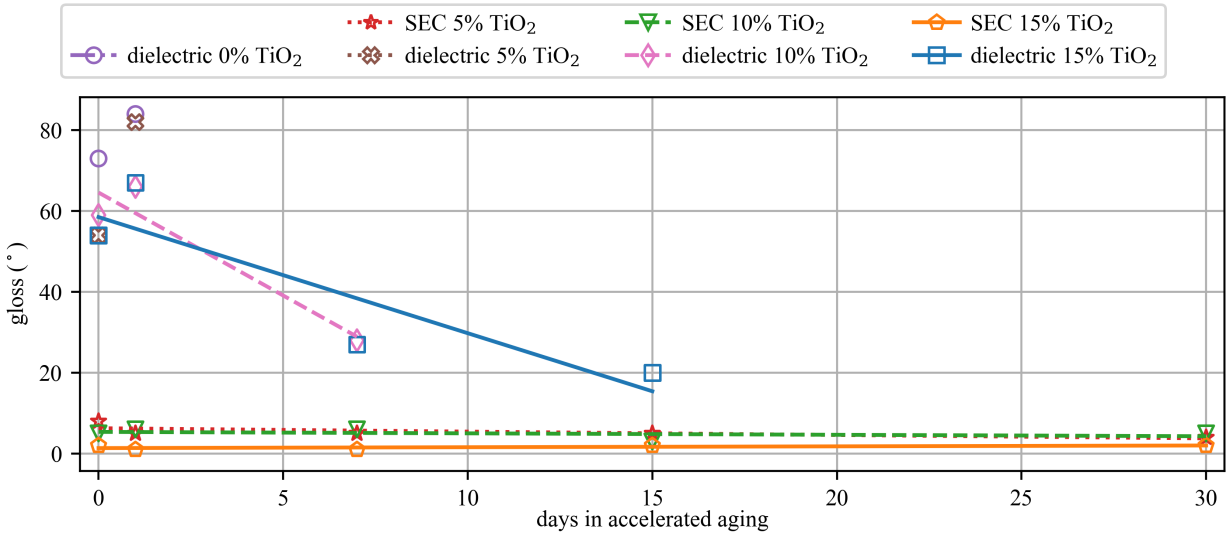

Figure 9: Colorimetry analysis of SECs and dielectrics with different levels of TiO_2 in the dielectric layer, after accelerated aging.

Table 2: Regression values for the measured tensile strengths at rupture (σ_r) presented in figure 6(a). [Note: "F": too fragile to implement mechanical test.]

sample	slope	r value	standard error
dielectric 0% TiO_2	F	F	F
dielectric 5% TiO_2	F	F	F
dielectric 10% TiO_2	F	F	F
dielectric 15% TiO_2	-0.329	-0.994	0.037
SEC 5% TiO_2	-0.003	-0.095	0.018
SEC 10% TiO_2	-0.005	-0.169	0.018
SEC 15% TiO_2	-0.004	-0.121	0.020

Table 3: Regression values for the measured strain at rupture (σ_r) presented in figure 6(b).

sample	slope	r value	standard error
dielectric 0% TiO_2	F	F	F
dielectric 5% TiO_2	F	F	F
dielectric 10% TiO_2	F	F	F
dielectric 15% TiO_2	-20.93	-0.94	7.45
SEC 5% TiO_2	-5.34	-0.58	4.27
SEC 10% TiO_2	-7.24	-0.61	5.36
SEC 15% TiO_2	-3.03	-0.24	7.14

to perform mechanical tests on: these samples are marked with an "F" in Tables 2 - 6". Additionally,

Table 4: Regression values for the calculated material modulus presented in figure 6(c).

sample	slope	r value	standard error
dielectric 0% TiO_2	F	F	F
dielectric 5% TiO_2	F	F	F
dielectric 10% TiO_2	F	F	F
dielectric 15% TiO_2	0.019	0.549	0.029
SEC 5% TiO_2	-0.014	-0.854	0.005
SEC 10% TiO_2	-0.015	-0.572	0.013
SEC 15% TiO_2	-0.021	-0.642	0.014

results for these fragile specimens are not presented in figure 6 or the following figures. Linear regression analysis is applied to the data sets with three or more data points and these results are tabulated in tables 2 - 4. Results show that the dielectric with 0% TiO_2 (pure SEBS) is very sensitive to the accelerated aging processes as demonstrated by reductions in the tensile strength and strain at rupture after just one day of accelerated aging. Using the pure SEBS dielectric as a reference, the addition of TiO_2 greatly improves the dielectric's durability, which is particularly observable with the strain at rupture. The SECs were found to be much more resilient to the accelerated aging than the dielectrics. The stability of the SECs' mechanical properties, even after 30 days of accelerated aging, are a prod-

uct of the protection provided by the carbon-black-based conductive layer found painted on top of the dielectric layer. Linear regression analysis of the SECs that experienced 30 days of accelerated aging shows a reduction of 20.5%, 17.2%, and 19.6% in the Young's modulus for the SECs with dielectrics made with 5%, 10%, and 15% TiO_2, respectively.

Table 5: Regression values for the measured residual masses presented in figure 7.

sample	slope	r value	standard error
dielectric 0% TiO_2	0	0	0.029
dielectric 5% TiO_2	-0.065	-0.487	0.067
dielectric 10% TiO_2	0.042	0.348	0.065
dielectric 15% TiO_2	0.117	0.503	0.116
SEC 5% TiO_2	-0.059	-0.641	0.041
SEC 10% TiO_2	0.05	0.464	0.055
SEC 15% TiO_2	0.006	0.038	0.09

Thermogravimetric analyses are presented in figure 7 in terms of residual mass values. From this figure, it can be seen that the higher percentages of TiO_2 in the dielectric correlate to the higher residual masses relative to specimens with lower levels of TiO_2. This phenomenon is most clearly seen for the dielectric with 15% TiO_2, whereby this formulation retained more than 40% of its mass while the dielectric with 0% TiO_2 retained about 1% of its mass. This higher residual mass is associated with the TiO_2. TiO_2 has been shown to perform well under high temperature thermogravimetric analysis in the order of 1000 °C [39], well above the maximum temperature of 800 °C used in the thermometric analysis. Aging does not influence the residual mass of any sample, as demonstrated by the low slope of the linear regression for each sample formulation, as tabulated in table 5.

4.3. Optical analysis

Figure 8 reports results from the spectrophotometer analysis. These results can be used to investigate the durability of the membranes by quantifying changes in solar reflectance due to the accelerated aging procedure. The relative change in solar reflectance is shown as the differences between the unaged specimens and the specimens (the dielectric layer and the SEC sensors) that were exposed to 1, 7, 15, and 30 days of accelerated aging. The SEC specimens performed significantly better

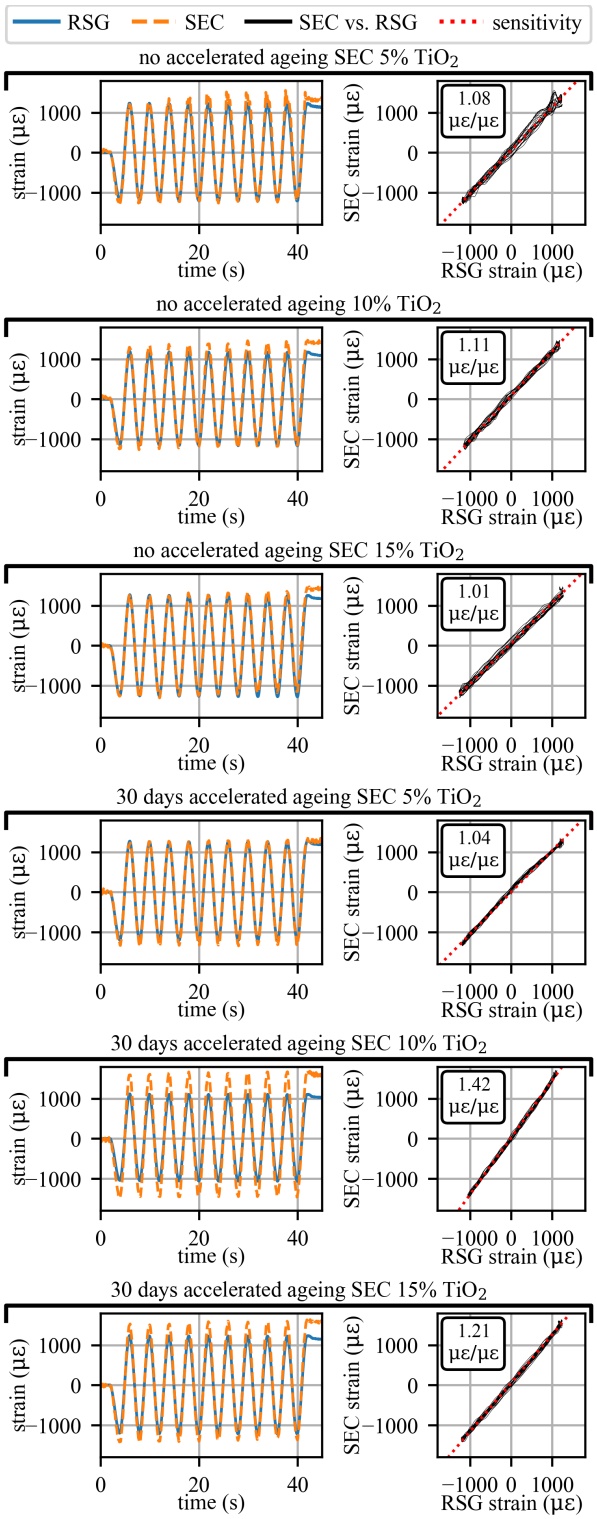

Figure 10: Temporal and sensitivity analysis for the SEC sensors without accelerated aging and with 30 days of accelerated aging.

Table 6: Regression values for the colorimetry analysis presented in figure 9.

sample	slope	r value	standard error
dielectric 0% TiO_2	F	F	F
dielectric 5% TiO_2	F	F	F
dielectric 10% TiO_2	-5.093	-0.953	1.611
dielectric 15% TiO_2	-2.872	-0.893	1.026
SEC 5% TiO_2	-0.083	-0.682	0.052
SEC 10% TiO_2	-0.036	-0.363	0.053
SEC 15% TiO_2	0.022	0.487	0.022

Table 7: Initial capacitance of control specimens and its variation after 12 months.

sensor no.	TiO_2 (%)	initial C (pF)	final C (pF)	change (%)
1	5	497	499	0.40
2	5	535	540	0.93
3	5	516	523	1.36
4	10	549	554	0.91
5	10	576	574	-0.35
6	10	537	545	1.49
7	15	528	527	-0.19
8	15	574	566	-1.39

than their dielectric counterparts in terms of their ability to maintain consistent optical characteristics during the weathering process. For the dielectric specimens, only the specimens that underwent 1 day of aging could be tested for each of the four TiO_2 concentration values. The specimens with an increased percentage (10 and 15%) of TiO_2 dispersed into the SEBS matrix could be tested after 7 days of accelerated aging. However, none of the dielectrics retained enough structural integrity to be tested after 15 and 30 days of accelerated aging. As shown in the right-hand column of figure 8, the SEC specimens appear to be more resilient to the accelerated aging tests. While exposed to the same accelerated aging tests as the dielectrics specimens, the SEC specimens retained a level of mechanical stability that allowed for spectrophotometer testing at each time interval. Testing showed that the SECs exhibited a much lower relative difference between the reference and the other specimens, (e.g., below

$$\pm$$

10% vs values higher than 12% for the dielectric specimens). This increase in durability, quantified by the lower relative difference, is a product of the carbon black doped outer electrode protecting the more sensitive dielectric. While the addition of the carbon black electrode shields the dielectric from direct solar reflectance measurements, it is interesting to note that the addition of titanium dioxide to the SEBS matrix seems to produce a higher spectral variation in the specimens. This spectral variation is particularly noticeable in the near infrared region (NIR) of the spectrum. Also of interest is the fact that the highest variations are generally associated with the specimens exposed to 1 and 15 days of accelerated aging. After 30 days of accelerated aging all the specimens show a reduced relative difference with respect to the neat sample. The SEC specimens produce a highly scattered behavior in the range 1700-2500 nm that is not present in the dielectric specimens: this is assumed to be a function of the addition of carbon black in the conductive electrodes.

Colorimetry analysis results are shown in figure 9 while the corresponding linear regression results are tabulated in table 6. The slope and standard error results for the measured gloss values quantitatively confirm that the color of the SEC sensor with 15% TiO_2 in the dielectric is the most stable, followed by the SEC sensor with 10% and 5% TiO_2. While the gloss stability of the SEC sensors is very high, the dielectric specimens do undergo a sharp drop in the measured gloss values due to the lack of protection provided by the conductive plates. The colorimetry analysis results data helps to further validate the stability provided by the carbon-black-based conductive plates to the accelerated weathering tests performed in this work.

4.4. Capacitance stability investigation

Tables 7 and 8 report the capacitance values for the SEC sensors over the one year investigation period. First, the aged control sensors are presented in table 7. These control sensors do not exhibit any clear reduction in capacitance with each sensor exhibiting no more than a 1.5% change in its capacitance. Due to the sensor being allowed to sit freely on the bench during testing, this value is well within the accuracy of the measurement system. Second, capacitance measurements for the SEC specimens that underwent the accelerated aging processes were recorded and tabulated in table

Table 8: Capacitance of SECs after QUV testing and 12 months of storage.

QUV (days)	TiO_2 (%)	initial C (pF)	final C (pF)	change (%)
0	5	520	513	-1.44
	10	583	563	-3.52
	15	540	525	-2.78
1	5	534	624	16.85
	10	581	510	-12.22
	15	545	534	-2.02
7	5	505	540	6.93
	10	586	558	-4.78
	15	558	550	-1.43
15	5	503	486	0.91
	10	546	568	4.03
	15	507	496	-2.17
30	5	481	482	0.21
	10	524	504	-3.82
	15	487	460	-5.54

8. These aged specimens do exhibit higher variations in their capacitance change over the 1 year period, however, these variations are not correlated to the extent of accelerated aging the specimens undertook. For example, the specimens that spent only 1 day in the QUV test chamber exhibited the highest variations (both positive and negative) in capacitance. A large source of these variations in capacitance can be attributed to the fact that the sensors' capacitance values were measured after material was removed for mechanical testing and as such the final C values in table 8 were extrapolated from specimens of reduced geometry. To expand, figure 2 shows the geometry of the SEC as measured for the capacitance stability investigation. The hypothesis that the source of the change in capacitance is a function of extrapolating capacitance values from the sensors after material is removed is further validated by the fact that when considering the sensors in the aged sample set, the total change for the average capacitance for all 15 sensors is a decrease of just 0.72% from their initial average capacitance.

4.5. Strain sensitivity analysis

Figure 10 reports the results for three control specimens and three specimens that underwent 30 days of accelerated aging for all three material formulations (5%, 10% and 15% TiO_2). These results present both the sensor's temporal response and their linearity with respect to the RSG. These results validated that the SEC specimens were still functioning after one year of storage and 30 days of accelerated aging. It can be noted that the SECs with 10% and 15% TiO_2 dispersed into the dielectric that underwent accelerated aging did experience an increase in their sensitivity. In comparison, the control SECs and the 5% TiO_2 SEC that underwent accelerated aging did not experience any notable change in their sensitivity. Overall, the SEC was shown to be relatively robust in terms of strain sensitivity, however, with accelerated aging some SECs with higher percentages of TiO_2 in the dielectric was found to have deviations in the sensitivity of the sensors. Future investigations will be required to both study and model the material degradation and its effect on the linearity of the SECs.

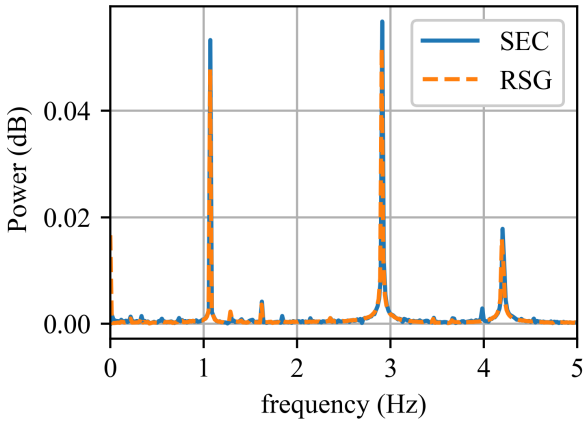

Figure 11: Power spectrum analysis of the SEC sensor removed from the South Skunk River Bridge.

Figure 11 reports the frequency results for the SEC removed from the South Skunk River Bridge. Results show that the SEC was capable of tracking the bridge's simulated frequency components, as verified by the RSGs. The average error in the power spectrum density between the SEC and RSG measured frequency components was for 0.422 mdB, for the frequency range from 0 to 5 Hz. During testing, the SEC was found to have a substantial temporal drift in its capacitance signal. It is the author's opinion that this drift is a function of prior manufacturing processes that caused the capacitor's electrodes to have lower levels of con-

ductivity. This substantial temporal drift does not manifest in the capacitance of the newer specimens, however, the effect of aging on the temporal drift in the SEC sensors will need to be investigated in future works.

5. Conclusion

The work investigated the long-term durability and weatherability of the SEC (soft elastomeric capacitor) sensors. The SEC is a strain transducing sensing skin that was developed for the monitoring of large scale structural components. The SEC is a parallel plate capacitor with the dielectric made of a styrene-ethylene-butylene-styrene (SEBS) block copolymer matrix filled with TiO_2 and two conductive plates consisting of the same SEBS matrix but doped with carbon black to increase its conductivity. The work presented here had the following findings: 1) the introduction of TiO_2 strongly improves the durability of the inner dielectric layer of the sensor; 2) the conductive plates doped with carbon black effectively act as protective layers for the inner dielectric; and 3) the SEC sensor kept its strain transducing ability throughout the studied lifespan. The increase in durability of both the SEC sensor and its dielectric layer was quantified through a series of mechanical, thermal, and optical tests. Additionally, it was demonstrated that the capacitance of the sensor does not significantly vary after aging and the SEC keeps its strain transducing properties. Results presented in this research demonstrate that when the dielectric of the SEC is doped with at least 5% TiO_2 the sensor is resilient to the effects of accelerated aging while keeping its mechanical, electrical, and strain transducing characteristics.

6. Acknowledgments

The support of the National Science Foundation Grant No. 1069283, which supports the activities of the Integrative Graduate Education and Research Traineeship (IGERT) in Wind Energy Science, Engineering and Policy (WESEP) at Iowa State University is gratefully acknowledged. This work is also partly supported by the Italian Ministry of Education, University and Research (MIUR) through the funded Project of Relevant National Interest (PRIN) entitled "SMART-BRICK: Novel strain-sensing nano-composite clay brick enabling self-monitoring masonry structures" (protocol no. 2015MS5L27). Any opinions, findings, and conclusions or recommendations expressed in this material are those of the authors and do not necessarily reflect the views of the funding agencies (National Science Foundation and MIUR).

[1] K. Worden, C. R. Farrar, G. Manson, G. Park, The fundamental axioms of structural health monitoring, Proceedings of the Royal Society A: Mathematical, Physical and Engineering Sciences 463 (2082) (2007) 1639–1664. doi:10.1098/rspa.2007.1834.
URL https://doi.org/10.1098/rspa.2007.1834

[2] D. H. Sigurdardottir, B. Glisic, On-site validation of fiber-optic methods for structural health monitoring: Streicker bridge, Journal of Civil Structural Health Monitoring 5 (4) (2015) 529–549. doi:10.1007/s13349-015-0123-x.
URL https://doi.org/10.1007/s13349-015-0123-x

[3] Y. Huang, X. Liang, S. A. Galedar, F. Azarmi, Integrated fiber optic sensing system for pipeline corrosion monitoring, in: Pipelines 2015, American Society of Civil Engineers, 2015. doi:10.1061/9780784479360.153.
URL https://doi.org/10.1061/9780784479360.153

[4] L. Gallucci, C. Menna, L. Angrisani, D. Asprone, R. S. L. Moriello, F. Bonavolontà, F. Fabbrocino, An embedded wireless sensor network with wireless power transmission capability for the structural health monitoring of reinforced concrete structures, Sensors 17 (11) (2017) 2566. doi:10.3390/s17112566.
URL https://doi.org/10.3390/s17112566

[5] B. Han, S. Sun, S. Ding, L. Zhang, X. Yu, J. Ou, Review of nanocarbon-engineered multifunctional cementitious composites, Composites Part A: Applied Science and Manufacturing 70 (2015) 69–81. doi:10.1016/j.compositesa.2014.12.002.
URL https://doi.org/10.1016%2Fj.compositesa.2014.12.002

[6] D. K. Hardy, M. F. Fadden, M. J. Khattak, A. Khattab, Development and characterization of self-sensing CNF HPFRCC, Materials and Structures 49 (12) (2016) 5327–5342. doi:10.1617/s11527-016-0863-z.
URL https://doi.org/10.1617/s11527-016-0863-z

[7] A. Downey, A. D'Alessandro, S. Laflamme, F. Ubertini, Smart bricks for strain sensing and crack detection in masonry structures, Smart Materials and Structures 27 (1) (2017) 015009. doi:10.1088/1361-665x/aa98c2.
URL https://doi.org/10.1088/1361-665x/aa98c2

[8] S. Luo, P. T. Hoang, T. Liu, Direct laser writing for creating porous graphitic structures and their use for flexible and highly sensitive sensor and sensor arrays, Carbon 96 (2016) 522–531. doi:10.1016/j.carbon.2015.09.076.
URL https://doi.org/10.1016/j.carbon.2015.09.076

[9] T. Schumacher, E. T. Thostenson, Development of structural carbon nanotube–based sensing composites for concrete structures, Journal of Intelligent Material Systems and Structures 25 (11) (2013) 1331–1339. doi:10.1177/1045389x13505252.
URL https://doi.org/10.1177/1045389x13505252

[10] M. Gerber, C. Weaver, L. Aygun, N. Verma, J. Sturm, B. Glišić, Strain transfer for optimal performance of sensing sheet, Sensors 18 (6) (2018) 1907. doi:10.3390/s18061907.

URL https://doi.org/10.3390/s18061907

[11] S. Laflamme, M. Kollosche, J. J. Connor, G. Kofod, Robust flexible capacitive surface sensor for structural health monitoring applications, Journal of Engineering Mechanics 139 (7) (2013) 879–885. doi:10.1061/(asce)em.1943-7889.0000530.
URL https://doi.org/10.1061/(asce)em.1943-7889.0000530

[12] V. A. Attarian, F. B. Cegla, P. Cawley, Long-term stability of guided wave structural health monitoring using distributed adhesively bonded piezoelectric transducers, Structural Health Monitoring: An International Journal 13 (3) (2014) 265–280. doi:10.1177/1475921714522842.
URL https://doi.org/10.1177/1475921714522842

[13] K. T. Wan, C. K. Leung, Durability tests of a fiber optic corrosion sensor, Sensors 12 (3) (2012) 3656–3668. doi:10.3390/s120303656.
URL https://doi.org/10.3390/s120303656

[14] H. Stoyanov, M. Kollosche, D. N. McCarthy, G. Kofod, Molecular composites with enhanced energy density for electroactive polymers, Journal of Materials Chemistry 20 (35) (2010) 7558. doi:10.1039/c0jm00519c.
URL https://doi.org/10.1039/c0jm00519c

[15] C. White, K. Tan, D. Hunston, T. Nguyen, D. Benatti, D. Stanley, J. Chin, Laboratory accelerated and natural weathering of styrene–ethylene–butylene–styrene (SEBS) block copolymer, Polymer Degradation and Stability 96 (6) (2011) 1104–1110. doi:10.1016/j.polymdegradstab.2011.03.003.
URL https://doi.org/10.1016/j.polymdegradstab.2011.03.003

[16] N. S. Allen, M. Edge, A. Wilkinson, C. M. Liauw, D. Mourelatou, J. Barrio, M. A. Martı'nez-Zaporta, Degradation and stabilisation of styrene–ethylene–butadiene–styrene (SEBS) block copolymer, Polymer Degradation and Stability 71 (1) (2000) 113–122. doi:10.1016/s0141-3910(00)00162-2.
URL https://doi.org/10.1016/s0141-3910(00)00162-2

[17] A. Ortiz-Negrón, D. Suleiman, The effect of TiO2nanoparticles on the properties of sulfonated block copolymers, Journal of Applied Polymer Science 132 (41) (2015) n/a–n/a. doi:10.1002/app.42651.
URL https://doi.org/10.1002/app.42651

[18] R. Day, The role of titanium dioxide pigments in the degradation and stabilisation of polymers in the plastics industry, Polymer Degradation and Stability 29 (1) (1990) 73–92. doi:10.1016/0141-3910(90)90023-z.
URL https://doi.org/10.1016/0141-3910(90)90023-z

[19] H. Saleem, M. Thunga, M. Kollosche, M. Kessler, S. Laflamme, Interfacial treatment effects on behavior of soft nano-composites for highly stretchable dielectrics, Polymer 55 (17) (2014) 4531–4537. doi:10.1016/j.polymer.2014.06.054.
URL https://doi.org/10.1016/j.polymer.2014.06.054

[20] E. Jubete, C. M. Liauw, K. Jacobson, N. S. Allen, Degradation of carboxylated styrene butadiene rubber based water born paints. part 1: Effect of talc filler and titania pigment on UV stability, Polymer Degradation and Stability 92 (8) (2007) 1611–1621. doi:10.1016/j.polymdegradstab.2007.04.016.
URL https://doi.org/10.1016/j.polymdegradstab.2007.04.016

[21] P. Latko, A. Bogucka, A. Boczkowska, Characterization of thermoplastic elastomers based composites doped with carbon black, Int J Mech Eng Autom 2 (2015) 171–176.

[22] J.-C. Huang, Carbon black filled conducting polymers and polymer blends, Advances in Polymer Technology 21 (4) (2002) 299–313. doi:10.1002/adv.10025.
URL https://doi.org/10.1002/adv.10025

[23] V. Zucolotto, J. Avlyanov, L. H. C. Mattoso, Elastomeric conductive composites based on conducting polymer-modified carbon black, Polymer Composites 25 (6) (2004) 617–621. doi:10.1002/pc.20056.
URL https://doi.org/10.1002/pc.20056

[24] M. Liu, A. Horrocks, Effect of carbon black on UV stability of LLDPE films under artificial weathering conditions, Polymer Degradation and Stability 75 (3) (2002) 485–499. doi:10.1016/s0141-3910(01)00252-x.
URL https://doi.org/10.1016/s0141-3910(01)00252-x

[25] S. Laflamme, F. Ubertini, H. Saleem, A. D'Alessandro, A. Downey, H. Ceylan, A. L. Materazzi, Dynamic characterization of a soft elastomeric capacitor for structural health monitoring, Journal of Structural Engineering 141 (8) (2015) 04014186. doi:10.1061/(asce)st.1943-541x.0001151.
URL https://doi.org/10.1061/(asce)st.1943-541x.0001151

[26] A. Wilkinson, M. Clemens, V. Harding, The effects of SEBS-g-maleic anhydride reaction on the morphology and properties of polypropylene/PA6/SEBS ternary blends, Polymer 45 (15) (2004) 5239–5249. doi:10.1016/j.polymer.2004.05.033.
URL https://doi.org/10.1016/j.polymer.2004.05.033

[27] X. Kong, J. Li, W. Collins, C. Bennett, S. Laflamme, H. Jo, A large-area strain sensing technology for monitoring fatigue cracks in steel bridges, Smart Materials and Structures 26 (8) (2017) 085024. doi:10.1088/1361-665x/aa75ef.
URL https://doi.org/10.1088/1361-665x/aa75ef

[28] A. Downey, S. Laflamme, F. Ubertini, Reconstruction of in-plane strain maps using hybrid dense sensor network composed of sensing skin, Measurement Science and Technology 27 (12) (2016) 124016. doi:https://doi.org/10.1088/0957-0233/27/12/124016.
URL http://stacks.iop.org/0957-0233/27/i=12/a=124016

[29] A. Downey, S. Laflamme, F. Ubertini, Experimental wind tunnel study of a smart sensing skin for condition evaluation of a wind turbine blade, Smart Materials and Structuresdoi:10.1088/1361-665X/aa9349.
URL https://doi.org/10.1088/1361-665X/aa9349

[30] S. Laflamme, M. Kollosche, V. D. Kollipara, H. S. Saleem, G. Kofod, Large-scale surface strain gauge for health monitoring of civil structures, in: A. L. Gyekenyesi (Ed.), Nondestructive Characterization for Composite Materials, Aerospace Engineering, Civil Infrastructure, and Homeland Security 2012, SPIE, 2012. doi:10.1117/12.913187.
URL https://doi.org/10.1117/12.913187

[31] W. Underground, Historical weather data for ames iowa municipal station, web site (Jan. 2018).
URL https://www.wunderground.com/history/monthly/us/ia/ames/KAMW

[32] Practice for fluorescent ultraviolet (UV) lamp apparatus exposure of plastics. doi:10.1520/d4329-99.
URL https://doi.org/10.1520/d4329-99

[33] Practice for operating fluorescent ultraviolet (UV) lamp apparatus for exposure of nonmetallic materials. doi:

10.1520/g0154-16.
URL https://doi.org/10.1520/g0154-16

[34] A. L. Pisello, E. Fortunati, C. Fabiani, S. Mattioli, F. Dominici, L. Torre, L. F. Cabeza, F. Cotana, PCM for improving polyurethane-based cool roof membranes durability, Solar Energy Materials and Solar Cells 160 (2017) 34–42. doi:10.1016/j.solmat.2016.09.036.

[35] K. Witt, Cie guidelines for coordinated future work on industrial colour-difference evaluation, Color Research & Application 20 (6) (1995) 399–403. doi:10.1002/col.5080200609.
URL https://doi.org/10.1002/col.5080200609

[36] Test method for solar absorptance, reflectance, and transmittance of materials using integrating spheres. doi:10.1520/e0903-96.
URL https://doi.org/10.1520/e0903-96

[37] Tables for reference solar spectral irradiances: Direct normal and hemispherical on 37 tilted surface. doi:10.1520/g0173-03r12.
URL https://doi.org/10.1520/g0173-03r12

[38] A. Pisello, Experimental analysis of cool traditional solar shading systems for residential buildings, Energies 8 (3) (2015) 2197–2210. doi:10.3390/en8032197.
URL https://doi.org/10.3390/en8032197

[39] B. Gao, G. Z. Chen, G. L. Puma, Carbon nanotubes/titanium dioxide (CNTs/TiO2) nanocomposites prepared by conventional and novel surfactant wrapping sol–gel methods exhibiting enhanced photocatalytic activity, Applied Catalysis B: Environmental 89 (3-4) (2009) 503–509. doi:10.1016/j.apcatb.2009.01.009.
URL https://doi.org/10.1016/j.apcatb.2009.01.009